The Journal of Chemical Physics ARTICLE pubs.aip.org/aip/jcp

Influence of atomistic features in plasmon–exciton coupling and charge transfer driven by a single molecule in a metallic nanocavity

Cite as: J. Chem. Phys. 161, 044707 (2024); doi: 10.1063/5.0216464
Submitted: 29 April 2024 • Accepted: 10 July 2024 •
Published Online: 31 July 2024

Bruno Candelas,[1,2,3,a)] Nerea Zabala,[1,2,3] Peter Koval,[4] Antton Babaze,[1,2] Daniel Sánchez-Portal,[1] and Javier Aizpurua[2,3,5,b)]

AFFILIATIONS

[1] Materials Physics Center, CSIC-UPV/EHU, Manuel de Lardizabal 5, 20018 Donostia, Spain
[2] Donostia International Physics Center, Manuel de Lardizabal 4, 20018 Donostia, Spain
[3] Department of Electricity and Electronics, FCT-ZTF, UPV/EHU, B° Sarriena s/n, 48940 Leioa, Spain
[4] Simune Atomistics S.L., Tolosa Hiribidea 76, 20018 Donostia, Spain
[5] IKERBASQUE, Basque Foundation for Science, 48009 Bilbao, Spain

Note: This paper is part of the JCP Special Topic on Plasmon-Mediated Nonlinear Optics and Dynamics.
[a)] **Electronic mail:** bcandelas001@ikasle.ehu.eus
[b)] **Author to whom correspondence should be addressed:** aizpurua@ehu.eus

ABSTRACT

When an organic molecule is placed inside a plasmonic cavity formed by two metallic nanoparticles (MNP) under illumination, the electronic excitations of the molecule couple to the plasmonic electromagnetic modes of the cavity, inducing new hybrid light–matter states called polaritons. Atomistic *ab initio* methods accurately describe the coupling between MNPs and molecules at the nanometer scale and allow us to analyze how atomistic features influence the interaction. In this work, we study the optical response of a porphine molecule coupled to a silver nanoparticle dimer from first principles, within the linear-response time-dependent density functional theory framework, using the recently developed Python Numeric Atomic Orbitals implementation to compute the optical excitations. The optical spectra show the splitting of the resonances of the plasmonic dimer and the molecule into two distinct polaritons, a characteristic feature of the strong light–matter coupling regime. Our results stress the importance of atomistic features, such as the gap configuration in determining the plasmon–exciton coupling strength and in the emergence of molecule-mediated charge-transfer plasmon (CTP) resonances at lower frequencies. Moreover, we show that the strength of the CTP resonance can be tuned by shifting the alignment of the molecular energy levels with respect to the Fermi level of the MNPs.

I. INTRODUCTION

The excitation of localized surface plasmons supported by metallic nanoparticles (MNPs) and dimers allows for an extreme localization of the induced electric field at optical frequencies, resulting in excellent optical nanocavities.[1] When a quantum emitter, such as an organic molecule, is placed inside an optical cavity, its electronic transitions (i.e., excitons) couple to the electromagnetic modes of the plasmonic cavity, which in the strong-coupling regime leads to the formation of hybrid light–matter modes called polaritons.[2,3] Under certain conditions, the emergence of these new modes allows for tuning the optical properties of the emitter. This has led to the proposal of many applications in the last few years in fields such as photochemistry,[4–6] single-photon emission,[7] electroluminescence,[8] and exciton transport,[9,10] among others.

The optical response of coupled molecule–MNP systems is usually described within the classical electrodynamics framework,[11] in which the electronic transitions of the molecules are often approximated by point dipoles, and plasmonic cavities are described with an appropriate dielectric formalism. Nevertheless, the extreme electromagnetic field localization allowed by nanoscale plasmonic cavities may result in the generation of a local inhomogeneous field experienced by the molecule. In such a situation, the point-dipole model subjected to a specific homogeneous field would fail to correctly capture the plasmon–exciton interaction.[12,13] Moreover, the classical description of the cavity is not able to address quantum phenomena arising at narrow gaps, such as spill in/out of the induced charge density at the interfaces,[14–17] or charge transfer between the MNPs and the molecule.[18,19] This has led to the development of a wide array of quantum models in the last few years.[20–22]

The aforementioned effects, which even quantum models struggle to properly capture, can be addressed with the use of quantum many-body frameworks,[23,24] which have proven to be a suitable tool to address molecule–MNP coupled systems in subnanometric cavities, when the system is small enough to be computationally affordable. Within time-dependent density functional theory (TDDFT), different approaches have been successfully implemented to describe quantum phenomena occurring in hybrid molecule–MNP systems, such as charge transfer,[25–27] or chemical enhancement in surface-enhanced Raman scattering.[28,29] Recent theoretical works have also reliably reproduced the strong-coupling regime between metallic clusters and molecules by first-principles modeling,[30–32] and calculations with simplified jellium models have also suggested that the molecule–MNP coupling can be significantly perturbed by quantum effects arising at sub-nanometric distances, such as the hybridization between the atomic orbitals of the molecule and the metal.[33] Furthermore, atomistic TDDFT methods naturally account for geometric features of the system, which show significant influence in the detailed optical response of extreme nano- and pico-cavities.[23,24,34]

In this study, we analyze the optical response of a molecule–MNP dimer system from an atomistic *ab initio* perspective within the linear-response TDDFT framework, using the efficient iterative technique implemented in the PyNAO (Python Numeric Atomic Orbitals) code,[35] which uses a basis set of atomic orbitals and norm-conserving pseudopotentials. This computational tool offers a fully quantum description of the optical response of a nanosystem incorporating all the aforementioned quantum phenomena together with the effect of the atomistic features of the system. We focus our analysis on the dependence of the optical response of a molecule–MNP dimer system on the presence of atomistic features for dimer gaps smaller than 2 nm, showing that the atomistic morphology of the cavity at these extreme dimensions significantly affects the coupling strength and that it determines the existence of charge-transfer modes. We also find that the molecule–MNP coupling can be quenched for certain atomistic configurations of the cavity due to the electronic coupling between molecular and metallic orbitals.

A. Description of the molecule–MNP system

The canonical system under study is a dimer formed by two Ag nanoparticles of 309 atoms each, and a porphine molecule placed between them, as shown in Figs. 1(a) and 1(b) for a tip-to-tip and facet-to-facet cluster gap configurations, respectively. We consider an icosahedral geometry for the Ag_{309} nanoparticles, which is a very stable configuration for small metallic clusters.[36] This particular molecule has been chosen because its main optical resonance at 3.4 eV matches the plasmonic resonance of the dimer, which allows for a very efficient electromagnetic molecule–MNP coupling. Furthermore, the approximate diameter of the MNPs is 2.2 nm (from tip to tip), which is at the meeting point between two different approaches followed in the literature of the last few decades, the bottom-up approach of atomic clusters and the top-down approach of small nanoparticles.[37] The diameter of the molecule is around 1 nm. With the aim of exploring all the different configurations, we modify the gap size D, defined as the minimal distance between atoms of different clusters, as well as its morphology, by changing the relative orientations of the MNPs. In the linear-response TDDFT calculations, the system is excited by a monochromatic plane wave polarized along the dimer axis direction (z axis). Due to the small size of the system, it is appropriate to assume a homogeneous incident electromagnetic field. Figures 1(c) and 1(d) show the ground-state total effective potential landscape of the system computed with atomistic *ab initio* DFT calculations, in which the atomic sites are clearly visible.

II. THEORY AND METHODS

In order to compute the optical response of the molecule–MNP system within the present linear-response TDDFT approach, we first obtain the ground state of the system in the Kohn–Sham scheme. We use the SIESTA[38,39] (Spanish Initiative for Electronic Simulations with Thousands of Atoms) software for these calculations, which utilizes norm-conserving pseudopotentials to effectively account for the removed core electrons. This allows us to naturally account for the effect of d-electrons of silver[40] by treating them as valence electrons and thus not including them in the pseudopotential. We employ the Generalized Gradient Approximation (GGA) proposed by Wu and Cohen for the exchange–correlation functional[41] and a double-ζ polarized (DZP) basis set of numerical atomic orbitals generated using an energy shift of 1 meV, in which the Kohn–Sham orbitals are expanded as a linear combination of atomic orbitals (LCAOs). The fineness of the real-space grid mesh used to compute the Hartree and exchange–correlation contributions to the energy and Hamiltonian corresponds to a plane wave cutoff of 250 Rydberg.

Then, we obtain the response of the system in the framework of linear-response TDDFT, in which the induced electron density in frequency domain, $\delta n(\mathbf{r};\ \omega)$, is given by integrating in space the product of a small perturbation of the external potential, δV_{ext}, with the interacting response function $\chi(\mathbf{r}, \mathbf{r}';\ \omega)$,

$$\delta n(\mathbf{r};\omega) = \int d^3\mathbf{r}'\ \chi(\mathbf{r},\mathbf{r}';\omega)\ \delta V_{ext}(\mathbf{r}';\omega), \tag{1}$$

or, equivalently, by using the response function of the non-interacting Kohn–Sham system χ_0 as

$$\delta n(\mathbf{r};\omega) = \int d^3\mathbf{r}'\ \chi_0(\mathbf{r},\mathbf{r}';\omega)\ \delta V_{eff}(\mathbf{r}';\omega), \tag{2}$$

where $\delta V_{eff} = \delta V_{ext} + \delta V_{Hxc}$, with δV_{Hxc} being the variation of the Hartree–exchange–correlation potential. The response function χ of

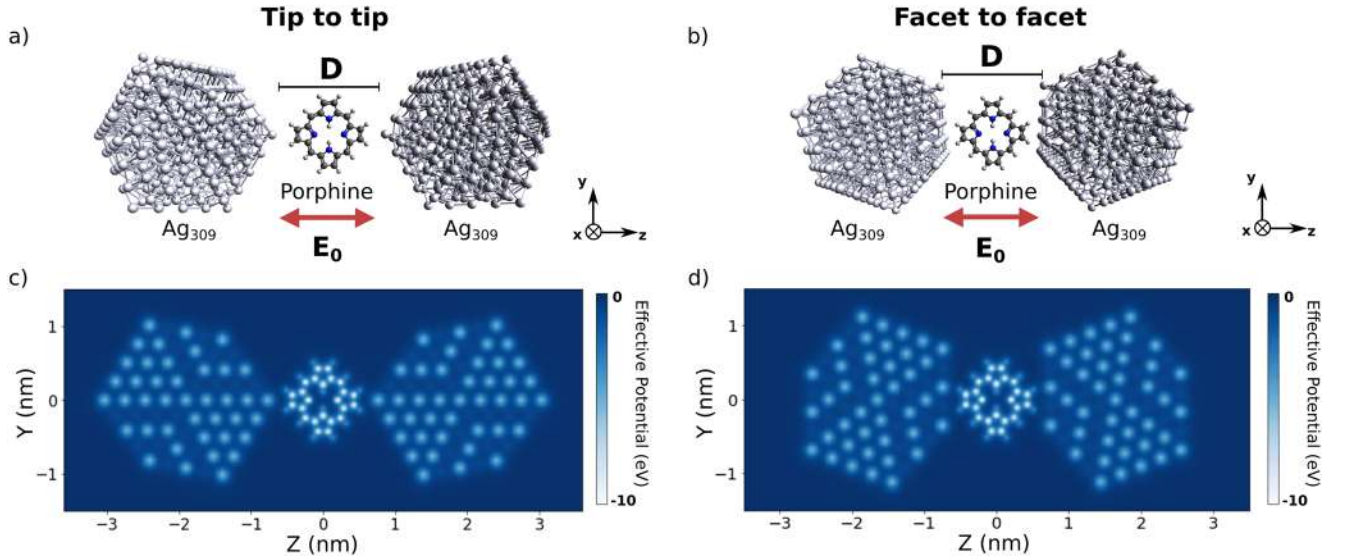

FIG. 1. (a) and (b) Representation of the canonical system under study in the tip-to-tip (a) and facet-to-facet (b) configurations. A porphine molecule is placed in the middle of the cavity formed by two silver icosahedral nanoparticles of 309 atoms each, and the system is excited by light polarized along the dimer axis direction (z axis). A gap size of D = 1.5 nm is considered in this figure, defined as the minimal distance between atoms of different clusters. (c) and (d) Total effective potential landscape V_{eff} of the ground state of the hybrid system for the $x = 0$ plane for the tip-to-tip (c) and the facet-to-facet (d) configurations. The effective potential shows minima at the atomic positions, which appear as bright dots in (c) and (d).

an interacting system is unknown, but the response function of the non-interacting electron system χ_0 can be explicitly expressed via products of Kohn–Sham eigenstates in the well-known Lehmann representation,

$$\chi_0(\mathbf{r},\mathbf{r}';\omega) = \sum_{n,m} (f_n - f_m)\ \frac{\phi_n^*(\mathbf{r})\phi_m(\mathbf{r})\phi_m^*(\mathbf{r}')\phi_n(\mathbf{r}')}{\omega - (E_m - E_n) + i\varepsilon}, \tag{3}$$

where ϕ_n are the Kohn–Sham wavefunctions, f_n are their corresponding occupation terms, and ε is an artificial Lorentzian spectral broadening, which phenomenologically accounts for the lifetime of the electronic excited states. In our calculations, we set the value of $\varepsilon = 0.05$ eV, which corresponds to a full width at half maximum of 0.1 eV. The response function χ_0 can then be used to compute the response of the real system using the following form of the Petersilka–Gossman–Gross equation[42] (where spatial variables are dropped for clarity):

$$[1 - K_{Hxc}(\omega)\ \chi_0(\omega)]\ \delta V_{eff}(\omega) = \delta V_{ext}(\omega), \tag{4}$$

in which K_{Hxc} is the Hartree–exchange–correlation kernel, defined as the variational derivative of the Hartree–exchange–correlation potential with respect to the density

$$K_{Hxc}(\omega) = \frac{\delta V_{Hxc}(\omega)}{\delta n(\omega)}. \tag{5}$$

Equation (4) gives the perturbation of the effective potential for an external perturbation δV_{ext}, which, for an optical excitation consisting of a monochromatic plane wave, can be expressed in the dipole approximation as $\delta V_{ext} = \mathbf{E_0}\cdot\mathbf{r}$, where $\mathbf{E_0}$ is the amplitude of the excitation field and $\mathbf{r}$ is the spatial position. Then, the induced density $\delta n(\mathbf{r};\ \omega)$ can be directly obtained from Eq. (2), which allows for the computation of the relevant quantities.

The previously described monochromatic plane wave excitation induces a variation in the density

$$\delta n(\mathbf{r};\omega) = \int d^3\mathbf{r}'\ \chi(\mathbf{r},\mathbf{r}';\omega)\ \mathbf{r}'\ \mathbf{E_0}, \tag{6}$$

and from this distribution, we can compute the induced dipole moment along the j direction as

$$p_j(\omega) = -\int d^3\mathbf{r}\ r_j\ \delta n(\mathbf{r};\omega). \tag{7}$$

The optical polarizability tensor of the system $\hat{\boldsymbol{\alpha}}(\omega)$ relates the external field to the induced dipole moment and is given by

$$\mathbf{p}(\omega) = \hat{\boldsymbol{\alpha}}(\omega)\ \mathbf{E_0}. \tag{8}$$

Finally, the absorption cross section, which describes the optical response of the system, can be extracted from the trace of the imaginary part of the polarizability as

$$\sigma_{abs}(\omega) = \frac{4\pi\omega}{c}\ \mathrm{Tr}\left[\mathrm{Im}\{\hat{\boldsymbol{\alpha}}(\omega)\}\right], \tag{9}$$

with c the speed of light. Since in this work we have only considered an excitation along the z direction (see Fig. 1), the absorption cross

section is directly proportional to Im $\{\alpha_{zz}\}$, which can be obtained from Eq. (8) as

$$\alpha_{zz}(\omega) = \int d^3\mathbf{r}\, d^3\mathbf{r}'\, z\, \chi(\mathbf{r},\mathbf{r}';\omega)\, z' \tag{10}$$

$$= \int d^3\mathbf{r}\, z\, \delta n(\mathbf{r};\omega), \tag{11}$$

where $\delta n(\mathbf{r};\ \omega)$ is the density response to an external monochromatic constant perturbation with $\mathbf{E_0} \propto [0,0,1]$.

The induced electric field in the frequency domain $\delta\mathbf{E}_{ind}(\mathbf{r};\ \omega)$ can be directly computed from the induced density as a Coulomb integral,

$$\delta\mathbf{E}_{ind}(\mathbf{r};\omega) = -\int \frac{\mathbf{r}-\mathbf{r}'}{|\mathbf{r}-\mathbf{r}'|^3}\, \delta n(\mathbf{r}';\omega)\, d^3\mathbf{r}'. \tag{12}$$

We perform the calculations described above with the PyNAO[35] software, which uses an effective iterative scheme to obtain the optical response within the adiabatic local-density approximation, employing a LCAO basis set. The efficiency of this method comes from solving iteratively Eq. (4) instead of using standard matrix inversion. This code has been proven to be a very efficient tool to compute the optical properties of small metallic clusters containing up to several hundreds of atoms and has already been successfully applied to the study of optical properties of silver and sodium clusters and dimers,[23,43,44] showing the role of single-atom features in optical cavities. More details on the implementation of the method are explained in Sec. II C of the supplementary material.

III. RESULTS AND DISCUSSION

A. Optical response of the isolated constituents

Before looking at the optical response of the coupled molecule–MNP system, it is instructive to address the behavior of the isolated constituents separately. In Fig. 2(a), we plot the absorption cross section (σ_{abs}) of a bare Ag_{309} dimer characterized by a gap size D = 1.5 nm for both the tip-to-tip and facet-to-facet configurations, together with the spectrum of the isolated molecule, as calculated within the linear-response TDDFT framework described in Sec. II. The spectrum of the dimer is dominated by a Bonding Dipole Plasmon (BDP) around 3.4 eV for both configurations. The nature of this mode is confirmed by the induced charge densities plotted in the inset of Fig. 2(a) and in Figs. 2(c) and 2(d), which reveal a dipolar pattern of the induced charge density at the surface of each MNP, characteristic of BDP excitations. The dipolar distributions of the induced charge density around the atomic sites are a signature of the atomistic response associated with the localized 3d orbitals of silver. The spectrum of the isolated molecule presents

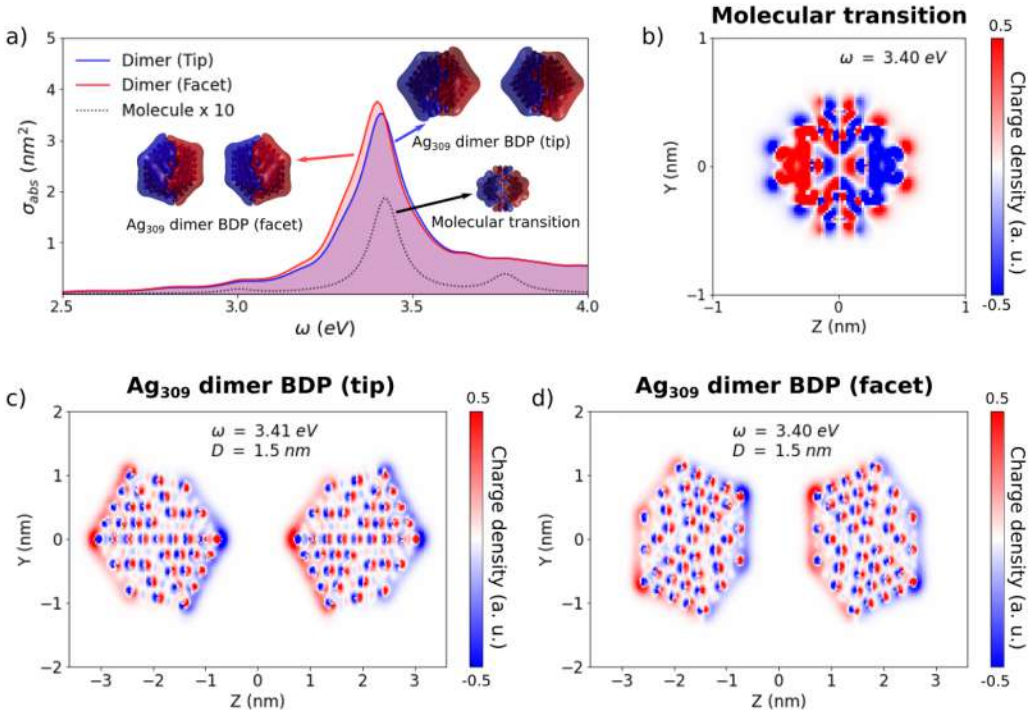

FIG. 2. (a) Optical absorption spectra of the bare silver dimer for a gap size D = 1.5 nm in the tip-to-tip (blue line) and facet-to-facet (red line) configurations and for the isolated porphine molecule (black dotted line). The insets show isosurfaces of induced charge density obtained with TDDFT at the resonance frequencies. (b) Snapshot of the induced charge density for the isolated molecule at resonance (ω = 3.40 eV). (c) Snapshot of the induced charge density for the bare tip-to-tip silver dimer with separation distance D = 1.5 nm at resonance (ω = 3.41 eV). (d) Snapshot of the induced charge density for the bare facet-to-facet silver dimer with separation distance D = 1.5 nm at resonance (ω = 3.40 eV).

a strong resonance around 3.4 eV overlapping with the BDP resonance of the dimer, which allows for an efficient coupling between the molecular and plasmonic resonances. The induced density plots in the inset of Fig. 2(a) and in Fig. 2(b) demonstrate that this resonance corresponds to the electronic excitonic dipolar transition of the molecule.

B. Optical response of the molecule–MNP coupled system

After analyzing the optical response of the isolated constituents, we study the effect of the optoelectronic coupling on the optical response of the molecule–MNP hybrid system. We first focus on the tip-to-tip configuration in order to describe the general behavior of the system and later study the influence of the cavity morphology on the coupling by comparing these results with those obtained in a facet-to-facet configuration. Figure 3(a) shows its absorption spectra for values of the gap size ranging from D = 1.4 nm (bottom) to D = 1.8 nm (top). Two distinct peaks well separated spectrally are clearly visible in all the spectra, which is a characteristic of strongly coupled systems. The lower polariton (LP) resonance, marked with yellow dots, is red-shifted with respect to the resonances of the bare dimer and the molecule, whereas the upper polariton (UP) resonance, marked with green dots, is blue-shifted. The splitting of the LP and UP peaks greatly depends on the gap size: for small values of D, they are clearly differentiated, but they merge gradually when the value of D is increased. This behavior indicates that the strength of the coupling between the molecular and plasmonic resonances decreases when increasing the separation distance, as the amplitude of the induced field decreases too.

The evolution of the spectra with the separation distance in Fig. 3(a) also shows that the UP remains almost stationary, while the LP experiences a significant redshift as the gap closes. The coupling of a single plasmonic mode and a single exciton should show a symmetric splitting of upper and lower polaritons; however, in our case, the small size of the gap enables the activation of higher-order plasmonic modes, which are responsible for the asymmetric evolution observed in Fig. 3(a). We have corroborated this aspect in Sec. II D of the supplementary material, by performing a classical calculation of the hybrid response of a molecule–plasmonic gap system of the same dimensions as those presented here, where a symmetric split is obtained when considering a single plasmonic mode and a similar asymmetric split is obtained when the full plasmonic response is adopted. Additional effects, such as the quenching of the molecular transition caused by the hybridization between the electronic states of the molecule and those of the MNPs,[45] could further produce a more pronounced asymmetry of polaritonic branches.

To get further insights into the nature of the hybrid polaritonic modes, we show in Fig. 3(b) the phase difference in the oscillations between the dipoles induced at the MNPs and at the molecule, which has been extracted by analyzing the real and imaginary parts of the induced density (see Sec. II E of the supplementary material). The values of this phase difference for each mode are displayed as a function of the gap distance D. In the LP, the MNPs and the molecule oscillate almost in phase, as observed in Fig. 3(c), which depicts the induced charge density for the LP mode in the D = 1.4 nm case. This behavior is maintained for the whole range of analyzed gap sizes. In the UP, in contrast, the pattern of oscillations is close to antiphase for the smallest gap size geometry, as shown by the induced charge

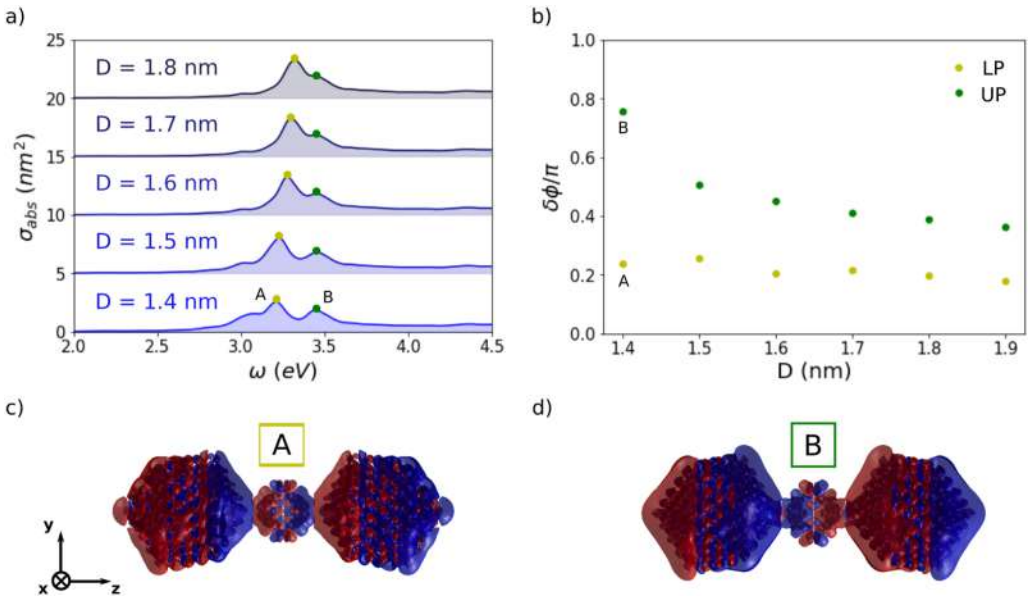

FIG. 3. (a) Optical absorption spectra of the hybrid molecule–MNP system for different gap sizes D. Spectra on the top correspond to large D values, and spectra on the bottom correspond to smaller D values. Yellow and green dots mark the LP and UP resonances, respectively. (b) Phase difference between the dipoles induced at the MNPs and at the molecule for both the LP and UP resonances as a function of the gap size D. (c) Isosurface of induced charge density for the LP resonance in the D = 1.4 nm geometry. (d) Isosurface of induced charge density for the UP resonance in the D = 1.4 nm geometry.

density depicted in Fig. 3(d). When the gap size increases, however, the phase difference falls to below $\pi/2$, which could be interpreted as an additional evidence of the diminishing coupling strength.

C. Influence of the cavity morphology

The distribution of the induced electric field inside a nanometric cavity is determined by the morphology of the cavity, specially by atomistic features, such as tips, edges, or facets.[46] To illustrate the dependence of the coupling between the dimer and the molecule on atomistic details, we have repeated the previous tip-to-tip calculations for the facet-to-facet configuration of the MNPs. We found in this case that, for the smallest value of the gap size considered in this work, D = 1.4 nm, the expected two-peak profile breaks up, with a third peak emerging between the LP and the UP resonances. This can be observed in Fig. 4(a), which shows the comparison between the absorption spectra for the tip-to-tip (blue line) and facet-to-facet (red line) configurations for D = 1.4 nm. We represent the corresponding atomistic structures in the insets. Figure 4(b) displays the isosurfaces of the induced charge density calculated for the three peaks in the absorption spectra. The one at 3.0 eV (A) shows a pattern of in-phase oscillations similar to the LP resonance of Fig. 3(c), whereas in the one at 3.45 eV (B), molecule and MNPs are nearly out-of-phase, as for the UP resonance in Fig. 3(d). For the resonance at 3.25 eV (C), visual inspection is not enough to identify the phase difference, but when the phase is computed from the induced density as described in Sec. II E of the supplementary material, the resulting value is close to $\pi/2$. For a complete description of the behavior of the facet-to-facet system, see the supplementary material, Fig. S2.

The emergence of this third peak between the LP and UP resonances in the facet-to-facet configuration is attributed to the hybridization between the electronic states of the molecule and the MNPs,[33,45,47] which provides an additional decay channel for the molecular excitation, decreases its lifetime, and causes a quenching of the signature of the molecular excitation in the absorption spectrum. Nevertheless, our calculations show that the double-peak structure in the absorption spectrum is recovered in the facet-to-facet configuration for larger D values (see the supplementary material, Fig. S2), with the splitting of the modes decreasing as the gap size increases, as in the tip-to-tip case.

A coupled molecule–MNP system is considered to be in the strong-coupling regime when the splitting of the emerging modes is larger than the losses of the system. We will refer to one of the most widely used criteria to identify the strong-coupling regime, which defines the following threshold for the coupling strength g:[48]

$$g \geq \frac{\gamma_{pl} + \gamma_{ex}}{4}, \tag{13}$$

where γ_{pl} and γ_{ex} are the losses of the BDP and the molecular excitation, respectively.

In our case, we obtain the values of $\gamma_{pl} = 0.191$ eV and $\gamma_{ex} = 0.107$ eV by fitting the absorption spectra of the isolated constituents to Lorentzian functions as described in Sec. II A of the supplementary material (the plasmonic losses vary slightly for the different dimer configurations considered, so we take the largest of them). Then, the value of g for the molecule–MNP system is estimated by fitting the absorption spectra of the hybrid system to a coupled-oscillator model[49] (see Sec. II A of the supplementary material). Figure 4(c) shows the values of the coupling strength g obtained for different gap sizes and for the two configurations of the MNPs considered in this work, ranging between 0.07 and 0.14 eV.

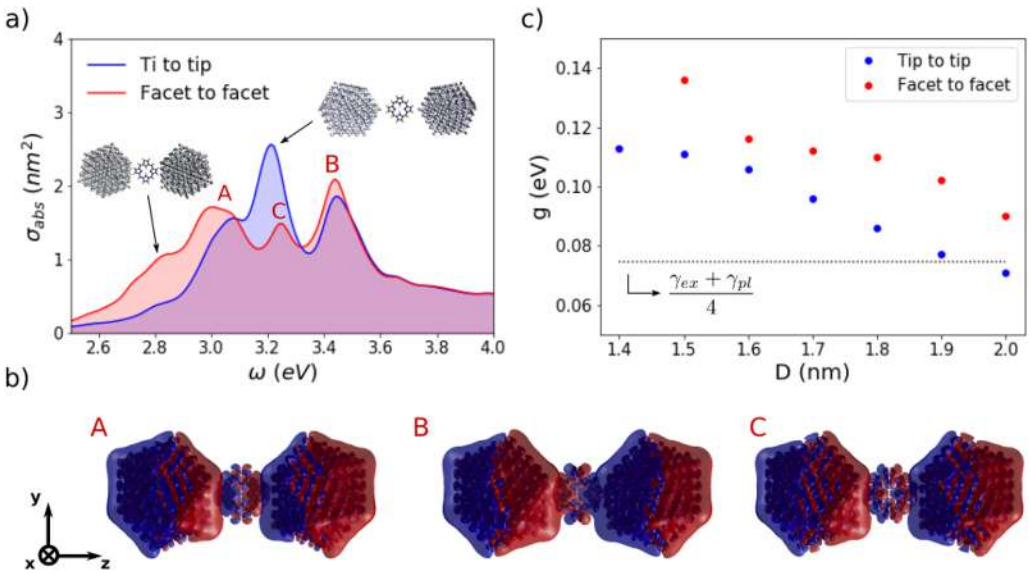

FIG. 4. (a) Comparison of absorption spectra for the tip-to-tip and facet-to-facet dimer configurations with D = 1.4 nm. The figures in the insets display the geometries of the tip-to-tip (blue line) and facet-to-facet (red line) configurations. The letters A, B, and C mark the three emerging modes at 3.0, 3.45, and 3.25 eV, respectively. (b) Induced charge densities at the resonance frequencies of the facet-to-facet geometry. (c) Values of the coupling strength g for both systems as a function of the gap size D. The black dotted line represents the threshold for strong coupling according to Eq. (13).

The strong-coupling condition, marked by the black dotted line in Fig. 4(c), is fulfilled for the whole range of considered gap sizes. The D = 1.4 nm case for the facet-to-facet configuration is omitted because its absorption spectrum does not show the characteristic two-peak behavior.

The facet-to-facet configuration consistently outperforms the tip-to-tip configuration, with a mean difference in coupling strength larger than 20%, confirming the influence of atomic features in setting up the plasmon–exciton interaction in the dimer cavity. This difference in the coupling strength is caused by the dissimilarity of the spatial distributions of the induced electric field for each configuration, as shown in Figs. 5(a) and 5(b). In the tip-to-tip case, the induced field is strongly localized around the vertices of the MNPs due to the atomistic lightning-rod effect,[46] whereas in the facet-to-facet case, it is more homogeneously distributed inside the cavity, enabling a more efficient coupling with the molecule. The final coupling strength is thus a consequence of the presence of sharp features, as well as of the existence of large extensions of field enhancement.

This conclusion is also supported by auxiliary estimations of the coupling strength from the induced electric fields for the bare dimer, as explained in Sec. II F of the supplementary material, which predict a larger coupling in the facet-to-facet configuration than in the tip-to-tip configuration, as illustrated in the supplementary material, Fig. S4.

1. Induced electric fields

The LP and UP modes also show clear differences in the induced electric fields, which can be directly obtained from the induced density using Eq. (12). In Fig. 5, we compare the enhancement of the electric field for the bare nanoparticle dimer at the BDP resonance and for the molecule–MNP system at both the LP and the

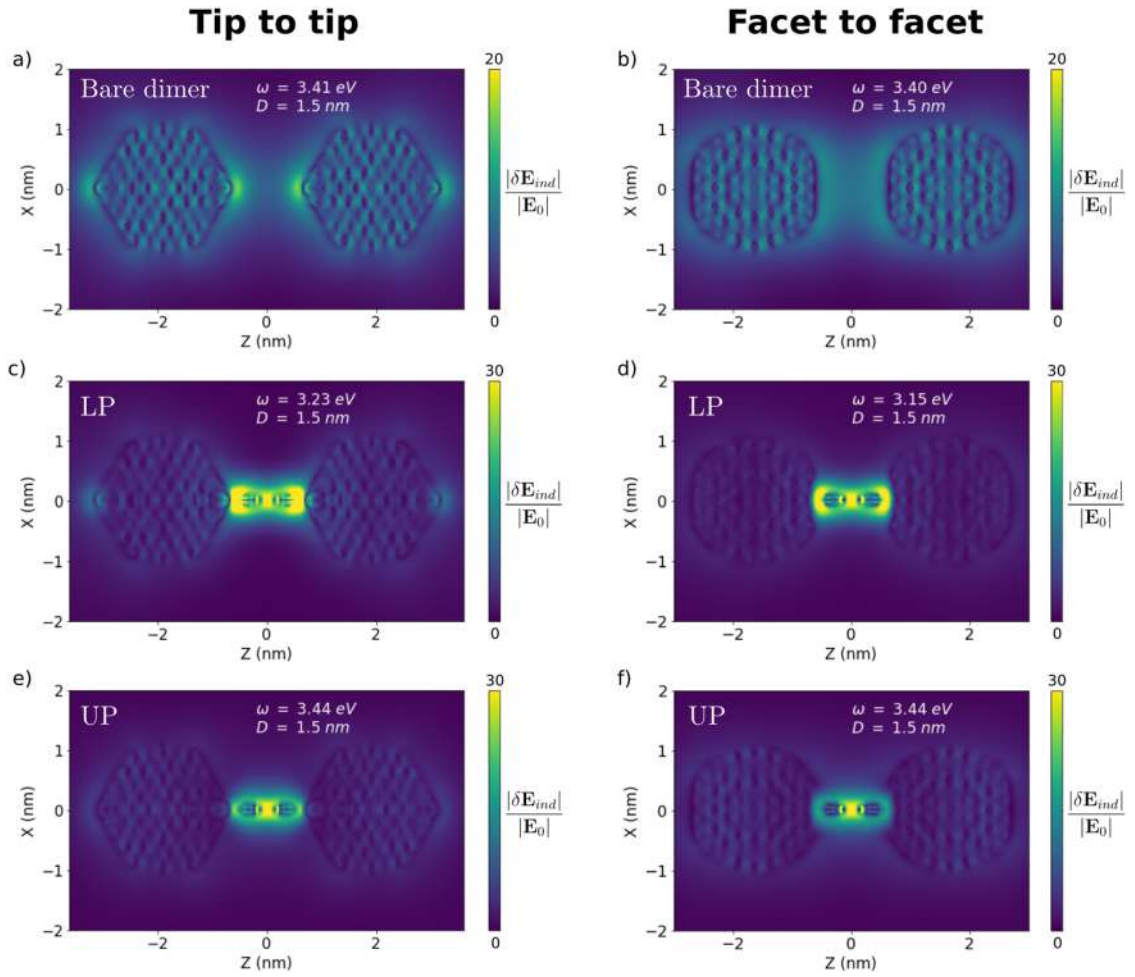

FIG. 5. (a) and (b) Electric field enhancement at the BDP resonance on the XZ plane for a bare nanoparticle dimer with gap size D = 1.5 nm for the tip-to-tip (a) and facet-to-facet (b) geometries. (c) and (d) Electric field enhancement on the XZ plane for the LP resonance of the tip-to-tip (c) and facet-to-facet (d) hybrid geometries with gap size D = 1.5 nm. (e) and (f) Electric field enhancement on the XZ plane for the UP resonance of the tip-to-tip (e) and facet-to-facet (f) hybrid geometries with gap size D = 1.5 nm.

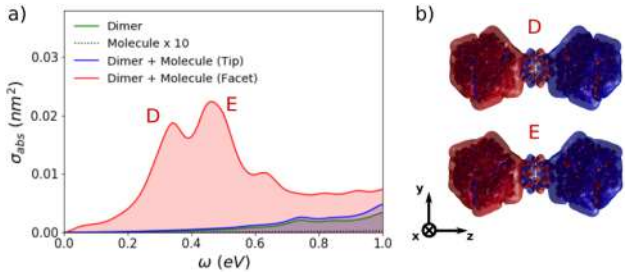

FIG. 6. (a) Low-energy part of the absorption spectrum for the bare dimer (green line), the isolated porphine molecule (black dotted line), and the hybrid system in both the tip-to-tip (blue line) and facet-to-facet (red line) configurations, with D = 1.4 nm. The emerging modes for the facet-to-facet configuration at 0.34 and 0.45 eV are marked as D and E, respectively. (b) Induced charge densities at the resonances D and E appearing for the facet-to-facet geometry.

UP resonances, for both the tip-to-tip and facet-to-facet configurations. As can be seen in Figs. 5(c) and 5(d), the induced field in the LP is distributed along the entire cavity and specially in the gap between the molecule and the MNPs, whereas the induced field in the UP, shown in Figs. 5(e) and 5(f), appears to be concentrated around the center of the molecule. A similar behavior has already been predicted in calculations with tetracene molecules and Mg nanoparticle dimers.[31] In both cases, the distribution of the field is drastically modified with respect to the BDP of the bare nanoparticle dimer depicted in Figs. 5(a) and 5(b). Despite the quantitative differences in the values of the coupling strength described previously (mainly due to the strength of the induced fields), the general qualitative properties of the induced field distributions of each polariton do not seem to be greatly influenced by the configuration of the cavity.

D. Charge-transfer plasmon

Following the analysis of the optical response of the molecule–MNP system and the nature of the characteristic resonances, we put now our focus on the low-energy range of the spectra. In Fig. 6(a), we show the absorption spectra of the hybrid system zoomed at the 0–1 eV range, in both the tip-to-tip (blue line) and the facet-to-facet (red line) configurations with D = 1.4 nm, together with the bare dimer (green line) and the isolated molecule (black dotted line) spectra. As observed, the cavity morphology plays a key role in the optical response at low energies. The isolated constituents do not exhibit any resonances in this frequency range, and the same occurs for the hybrid system in the tip-to-tip configuration. However, in the facet-to-facet configuration, a series of new peaks emerge at low energies. To get deeper insights into these low-energy resonances, we plot the corresponding induced charge densities in Fig. 6(b). The two main resonances, labeled D and E, display clear monopolar patterns on the surface of the MNPs, meaning that the individual MNPs are charged with opposite charge signs. This is a signature of the flow of charge from one cluster to the other through

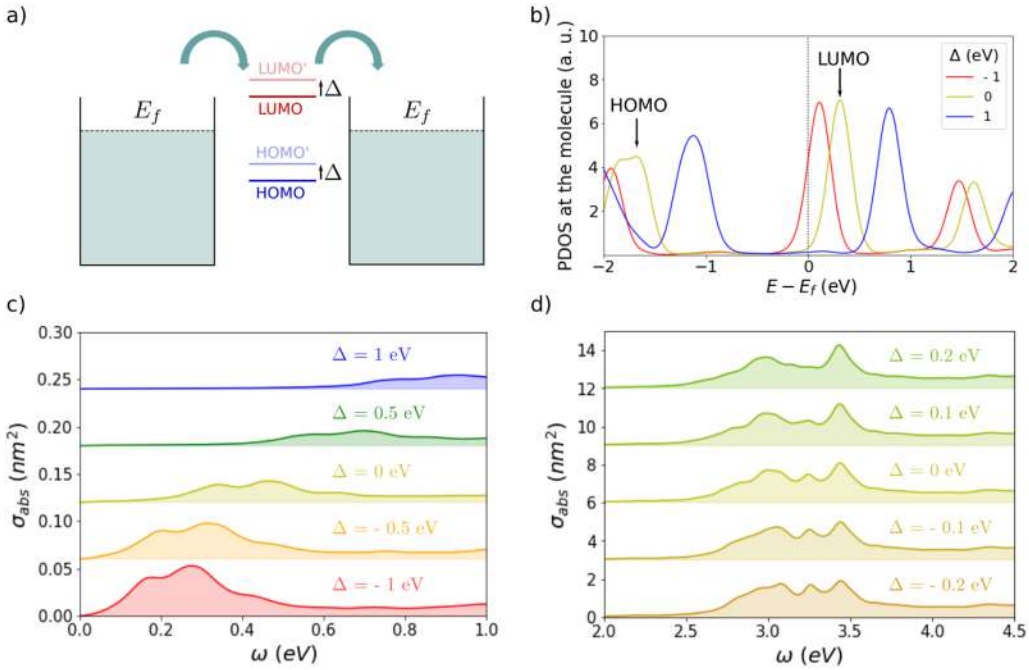

FIG. 7. (a) Sketch illustrating the energy shifting Δ of the HOMO and LUMO molecular energy levels with respect to the metal Fermi energy E_f. (b) Projected density of electronic states (PDOS) of the molecule around the Fermi level for different values of the energy shift Δ. The black dotted line stands for the Fermi level of the MNPs, and the HOMO and the LUMO are indicated for the Δ = 0 case. (c) Absorption spectrum of the system at CTP energies for different values of the energy shift Δ ranging from −1 eV (bottom) to 1 eV (top). (d) Absorption spectrum of the system at higher energies for values of the energy shift ranging from −0.2 eV (bottom) to 0.2 eV (top).

the molecular junction, which suggests the identification of charge-transfer plasmon (CTP) modes.[50] Since both modes are CTPs, the isosurfaces of induced charge density look very similar, with the main differences being localized at the molecule.

E. Shift of the molecular energy levels

It is well known that, for a molecule placed between two MNPs, the existence of molecular states close to the Fermi level of the MNPs triggers the electron conductivity of the system, which makes the intensity of CTP resonances very sensitive to the relative position of the molecular energy levels.[26] In practice, the relative position of these levels can be shifted by applying an external potential, as in single-molecule resonant tunneling experiments.[51] In the present atomistic *ab initio* framework, it is possible to shift these energy levels in a controlled way by introducing a background potential localized around the atomic sites of the molecule. Taking advantage of this possibility, we analyze the effect of a controlled shift of the molecular energy levels on the optical absorption of the system, as depicted in Fig. 7(a). The details of the implementation of this molecular energy shift are described in Sec. II G of the supplementary material. Since we are interested in the charge-transfer regime, all the calculations in this subsection are performed for the D = 1.4 nm case in the facet-to-facet configuration. In Fig. 7(b), we show the projected density of states (PDOS) at the molecule for different values of the energy shift Δ, choosing the Fermi level of the MNPs as the zero-energy reference. For Δ = 0 eV (i.e., when no shift is introduced), the highest occupied molecular orbital (HOMO) and the lowest unoccupied molecular orbital (LUMO) are localized around −1.6 and 0.4 eV, respectively. We analyze the energetics of the LUMO in the molecule as it holds the main role in charge transport.

In Fig. 7(c), we compare the low-energy part of the absorption spectra for the range of Δ values presented in Fig. 7(b) with the negative values at the bottom and the positive ones at the top. As can be observed in Fig. 7(b), negative Δ values shift the LUMO closer to the Fermi level of the MNPs, strengthening the intensity of the CTP resonances in Fig. 7(c). For positive Δ values, the opposite occurs: the LUMO shifts to higher energies, increasing its energy separation with respect to the Fermi level, which leads to a weakening of the CTP modes in the absorption spectrum.

Together with this variation of the intensity of the CTP modes, the shift of the molecular levels also results in a displacement of the CTP resonances. Figure 7(c) clearly shows that the CTP modes are red-shifted for negative Δ values and blue-shifted for positive values. As described above, this is explained by the change in the energy gap between the LUMO and the Fermi level of the MNPs, which increases for positive Δ values and decreases for negative ones.

It is also interesting to look at the influence of the molecular energy level shift Δ on the higher-energy part of the absorption spectrum, which we show in Fig. 7(d). As one can see, positive values of Δ as small as 0.2 eV remove the middle resonance [labeled as C in Fig. 4(a)], while negative Δ values increase the height of this peak, which suggests a connection with the charge transfer through the molecule.

IV. CONCLUSIONS

In this work, we have described the optical response of a porphine molecule coupled to an Ag_{309} dimer within an *ab initio* atomistic linear-response TDDFT framework. Our results show the splitting of the plasmonic resonance of the dimer into two clearly distinct polaritons, confirming that the system is at the strong-coupling regime for gap sizes smaller than 2 nm. A comparison of the coupling strength g values for the different gap geometries demonstrates that the atomistic configuration has a significant effect on the coupling strength, as the more homogeneous induced fields of the facet-to-facet configuration result in larger g values. The optical responses obtained for different dimer configurations prove that atomistic features also have a crucial influence on the emergence of CTPs at low frequencies, which, for our system, only appear in the facet-to-facet configuration. Therefore, our results stress the importance of the effects caused by atomistic details in the response of molecule–MNP coupled systems. We have also performed an analysis of the CTP modes emerging at low frequencies and have shown that their intensity and spectral position can be tuned by shifting the position of the molecular energy levels with respect to the Fermi level of the MNPs, which provides valuable insights into the mechanism behind charge-transfer phenomena. These results demonstrate the suitability of the employed TDDFT method for addressing the coupling between molecules and MNPs while simultaneously accounting for the influence of the atomistic configuration and quantum effects arising at narrow gaps and thus further consolidate atomistic *ab initio* methods as a feasible tool to describe the most extreme cases of quantum emitter–nanocavity interaction.

SUPPLEMENTARY MATERIAL

The supplementary material contains figures with the absorption spectra for the facet-to-facet configuration and for the bare dimers in the tip-to-tip configuration. It also includes theoretical background expanding the description of the TDDFT method, as well as explaining the coupled dipole model used to fit the absorption spectra, calculations of the absorption spectrum for an analogous classical system, the computation of the phase difference shown in Fig. 3(b), the implementation of the molecular energy level shift used to tune intensity of the charge-transfer plasmon resonance, and the method used for estimating the coupling strength from the induced electric fields of the bare dimers.

ACKNOWLEDGMENTS

B.C. thanks Marc Barbry for his help as a maintainer of the PyNAO code and his valuable advice. B.C. acknowledges support through the Ph.D. Student program of Materials Physics Center and Donostia International Physics Center. We also acknowledge support through Grant No. IT 1526-22 funded by the Department of Education, Research and Universities of the Basque Government, and Grant No. PID2022-139579NB-I00 funded by MCIN/AEI/10.13039/501100011033 and by "ERDF A way of making Europe". D.S.-P. acknowledges support through Grant No. IT 1569-22 funded by the Department of Education, Research and Universities of the Basque Government and Grant No. PID2022-140845OB-C66 funded by MCIN/AEI/10.13039/501100011033 and by "ERDF A way of making Europe."

AUTHOR DECLARATIONS

Conflict of Interest

The authors have no conflicts to disclose.

Author Contributions

Bruno Candelas: Conceptualization (equal); Formal analysis (lead); Investigation (lead); Software (lead); Visualization (lead); Writing – original draft (lead); Writing – review & editing (equal). **Nerea Zabala**: Conceptualization (equal); Supervision (equal); Writing – review & editing (equal). **Peter Koval**: Software (equal); Writing – review & editing (supporting). **Antton Babaze**: Formal analysis (supporting); Investigation (supporting); Writing – review & editing (equal). **Daniel Sánchez-Portal**: Conceptualization (equal); Software (equal); Writing – review & editing (equal). **Javier Aizpurua**: Conceptualization (equal); Supervision (equal); Writing – review & editing (equal).

DATA AVAILABILITY

The data that support the findings of this study are available from the corresponding author upon reasonable request. The SIESTA and PyNAO codes are available in Refs. 35 and 38. The dataset corresponding to the results shown in the figures of this paper can be found at https://digital.csic.es/.

REFERENCES

[1] M. Pelton, J. Aizpurua, and G. Bryant, "Metal-nanoparticle plasmonics," Laser Photonics Rev. **2**, 136–159 (2008).

[2] P. Törmä and W. L. Barnes, "Strong coupling between surface plasmon polaritons and emitters: A review," Rep. Prog. Phys. **78**(1), 013901 (2015).

[3] F. J. García-Vidal, C. Ciuti, and T. W. Ebbesen, "Manipulating matter by strong coupling to vacuum fields," Science **373**, eabd0336 (2021).

[4] F. Herrera and F. C. Spano, "Cavity-controlled chemistry in molecular ensembles," Phys. Rev. Lett. **116**, 238301 (2016).

[5] J. Galego, F. J. García-Vidal, and F. Feist, "Suppressing photochemical reactions with quantized light fields," Nat. Commun. **7**, 13841 (2016).

[6] Y. Kim, A. Barulin, S. Kim, L. P. Lee, and I. Kim, "Recent advances in quantum nanophotonics: Plexcitonic and vibro-polaritonic strong coupling and its biomedical and chemical applications," Nanophotonics **12**, 413–439 (2023).

[7] T. B. Hoang, G. M. Akselrod, and M. H. Mikkelsen, "Ultrafast room-temperature single photon emission from quantum dots coupled to plasmonic nanocavities," Nano Lett. **16**, 270–275 (2016).

[8] K. Miwa, S. Sakamoto, and A. Ishizaki, "Control and enhancement of single-molecule electroluminescence through strong light–matter coupling," Nano Lett. **23**, 3231–3238 (2023).

[9] J. Schachenmayer, C. Genes, E. Tignone, and G. Pupillo, "Cavity-enhanced transport of excitons," Phys. Rev. Lett. **114**, 196403 (2015).

[10] M. Wang *et al.*, "Plasmonic phenomena in molecular junctions: Principles and applications," Nat. Rev. Chem **6**, 681–704 (2022).

[11] P. Anger, P. Bharadwaj, and L. Novotny, "Enhancement and quenching of single-molecule fluorescence," Phys. Rev. Lett. **96**, 113002 (2006).

[12] T. Neuman, R. Esteban, D. Casanova, F. J. Carcía-Vidal, and J. Aizpurua, "Coupling of molecular emitters and plasmonic cavities beyond the point-dipole approximation," Nano Lett. **18**, 2358–2364 (2018).

[13] Y. Zhang, Z. C. Dong, and J. Aizpurua, "Influence of the chemical structure on molecular light emission in strongly localized plasmonic fields," J. Phys. Chem. C **124**, 4674–4683 (2020).

[14] M. Brack, "The physics of simple metal clusters: Self-consistent jellium model and semiclassical approaches," Rev. Mod. Phys. **65**, 677 (1993).

[15] G. Toscano, J. Straube, A. Kwiatkowski, C. Rockstuhl, F. Evers, H. Xu, N. A. Mortensen, and M. Wubs, "Resonance shifts and spill-out effects in self-consistent hydrodynamic nanoplasmonics," Nat. Commun. **6**, 7132 (2015).

[16] T. V. Teperik, P. Nordlander, J. Aizpurua, and A. G. Borisov, "Robust subnanometric plasmon ruler by rescaling of the nonlocal optical response," Phys. Rev. Lett. **110**, 263901 (2013).

[17] A. Babaze, E. Ogando, P. E. Stamatopoulou, C. Tserkezis, N. A. Mortensen, J. Aizpurua, A. G. Borisov, and R. Esteban, "Quantum surface effects in the electromagnetic coupling between a quantum emitter and a plasmonic nanoantenna: Time-dependent density functional theory vs. semiclassical feibelman approach," Opt. Express **30**(12), 21159–21183 (2022).

[18] J. Zuloaga, E. Prodan, and P. Nordlander, "Quantum description of the plasmon resonances of a nanoparticle dimer," Nano Lett. **9**, 887–891 (2009).

[19] D. C. Marinica, A. K. Kazansky, P. Nordlander, J. Aizpurua, and A. G. Borisov, "Quantum plasmonics: Nonlinear effects in the field enhancement of a plasmonic nanoparticle dimer," Nano Lett. **12**, 1333–1339 (2012).

[20] M. Sánchez-Barquilla, A. I. Fernández-Domínguez, J. Feist, and F. J. García-Vidal, "A theoretical perspective on molecular polaritonics," ACS Photonics **9**, 1830–1841 (2022).

[21] M. Ruggentahler, D. Sidler, and A. Rubio, "Understanding polaritonic chemistry from ab initio quantum electrodynamics," Chem. Rev. **123**, 11191–11229 (2023).

[22] G. Parolin, N. Peruffo, F. Mancin, E. Collini, and S. Corni, "Molecularly detailed view of strong coupling in supramolecular plexcitonic nanohybrids," Nano Lett. **24**, 2273–2281 (2024).

[23] M. Barbry, P. Koval, F. Marchesin, R. Esteban, A. G. Borisov, J. Aizpurua, and D. Sánchez-Portal, "Atomistic near-field nanoplasmonics: Reaching atomic-scale resolution in nanooptics," Nano Lett. **15**, 3410–3419 (2015).

[24] P. Zhang, J. Feist, A. Rubio, P. García-González, and F. J. García-Vidal, "*Ab initio* nanoplasmonics: The impact of atomic structure," Phys. Rev. B **90**, 161407 (2014).

[25] P. Song, P. Nordlander, and S. Gao, "Quantum mechanical study of the coupling of plasmon excitations to atomic-scale electron transport," J. Chem. Phys. **134**, 074701 (2011).

[26] V. Kulkarni and A. Manjavacas, "Quantum effects in charge transfer plasmons," ACS Photonics **2**, 987–992 (2015).

[27] A. S. Fedorov, M. A. Visotin, A. V. Lukyanenko, V. S. Gerasimov, and A. S. Aleksandrovsky, "Intense charge transfer plasmons in golden nanoparticle dimers connected by conductive molecular linkers," J. Chem. Phys. **160**, 084110 (2024).

[28] L. Jensen, C. M. Aikens, and G. C. Schatz, "Electronic structure methods for studying surface-enhanced Raman scattering," Chem. Soc. Rev. **37**, 1061–1073 (2008).

[29] S. Corni and J. Tomasi, "Theoretical evaluation of Raman spectra and enhancement factors for a molecule adsorbed on a complex-shaped metal particle," Chem. Phys. Lett. **342**(1–2), 135–140 (2001).

[30] T. P. Rossi, T. Shegai, P. Erhart, and T. J. Antosiewicz, "Strong plasmon-molecule coupling at the nanoscale revealed by first-principles modeling," Nat. Commun. **10**, 13336 (2019).

[31] M. Kuisma, B. Rousseaux, K. M. Czajkowski, T. P. Rossi, T. Shegai, P. Erhart, and T. J. Antosiewicz, "Ultrastrong coupling of a single molecule to a plasmonic nanocavity: A first-principles study," ACS Photonics **9**, 1065–1077 (2022).

[32] K. Kluczyk-Korch and T. J. Antosiewicz, "Hot carrier generation in a strongly coupled molecule-plasmonic nanoparticle system," Nanophotonics **12**(9), 1711–1722 (2023).

[33] A. Babaze, R. Esteban, A. G. Borisov, and J. Aizpurua, "Electronic exciton–plasmon coupling in a nanocavity beyond the electromagnetic interaction picture," Nano Lett. **21**, 8466–8473 (2021).

[34] A. Varas, P. García-González, F. J. García-Vidal, and A. Rubio, "Anisotropy effects on the plasmonic response of nanoparticle dimers," J. Phys. Chem. Lett. **6**, 1891–1898 (2015).

[35] P. Koval, M. Barbry, and D. Sánchez-Portal, "PySCF-NAO: An efficient and flexible implementation of linear response time-dependent density functional theory with numerical atomic orbitals," Comput. Phys. Commun. **236**, 188–204 (2019).

[36] Y. He and T. Zeng, "First-principles study and model of dielectric functions of silver nanoparticles," J. Phys. Chem. C **114**, 18023–18030 (2010).

[37] J. A. Scholl, A. L. Koh, and J. A. Dionne, "Quantum plasmon resonances of individual metallic nanoparticles," Nature **483**, 421–427 (2012).

[38] J. M. Soler, E. Artacho, J. D. Gale, A. García, J. Junquera, P. Ordejón, and D. Sánchez-Portal, "The SIESTA method for *ab initio* order-*N* materials simulation," J. Phys.: Condens. Matter **14**(11), 2745 (2002).

[39] A. García *et al.*, "Siesta: Recent developments and applications," J. Chem. Phys. **152**, 204108 (2020).
[40] S. Raza, N. Stenger, S. Kadkhodazadeh, S. V. Fischer, N. Kostesha, A. Jauho, A. Burrows, M. Wubs, and N. A. Mortensen, "Blueshift of the surface plasmon resonance in silver nanoparticles studied with EELS," Nanophotonics **2**, 131–138 (2013).
[41] Z. Wu and R. E. Cohen, "More accurate generalized gradient approximation for solids," Phys. Rev. B **73**, 235116 (2006).
[42] M. Petersilka, U. J. Grossmann, and E. K. U. Gross, "Excitation energies from time-dependent density-functional theory," Phys. Rev. Lett. **76**, 1212 (1996).
[43] P. Koval, F. Marchesin, D. Foerster, and D. Sánchez-Portal, "Optical response of silver clusters and their hollow shells from linear-response TDDFT," J. Phys.: Condens. Matter **28**(21), 214001 (2016).
[44] F. Marchesin, P. Koval, M. Barbry, J. Aizpurua, and D. Sánchez-Portal, "Plasmonic response of metallic nanojunctions driven by single atom motion: Quantum transport revealed in optics," ACS Photonics **3**, 269–277 (2016).
[45] D. C. Marinica, H. Luorenço-Martins, J. Aizpurua, and A. G. Borisov, "Plexciton quenching by resonant electron transfer from quantum emitter to metallic nanoantenna," Nano Lett. **13**, 5972–5978 (2013).
[46] M. Urbieta, M. Barbry, Y. Zhang, D. Sánchez-Portal, N. Zabala, and J. Aizpurua, "Atomic-scale lightning rod effect in plasmonic picocavities: A classical view to a quantum effect," ACS Nano **12**, 585–595 (2018).
[47] P. Garcia-Gonzalez, A. Varas, F. J. Garcia-Vidal, and A. Rubio, "Single-atom control of the optoelectronic response in sub-nanometric cavities," arXiv:1903.08443 (2019).
[48] G. Khitrova, H. M. Gibbs, M. Kira, S. W. Koch, and S. Scherer, "Vacuum Rabi splitting in semiconductors," Nat. Phys. **2**, 81–90 (2006).
[49] X. Wu, S. K. Gray, and M. Pelton, "Quantum-dot-induced transparency in a nanoscale plasmonic resonator," Opt. Express **18**, 23633 (2010).
[50] O. Pérez-González, N. Zabala, A. G. Borisov, N. J. Halas, N. Nordlander, and J. Aizpurua, "Optical spectroscopy of conductive junctions in plasmonic cavities," Nano Lett. **10**, 3090–3095 (2010).
[51] M. L. Perrin, E. Galan, R. Eelkema, F. Grozema, J. M. Thijssen, and H. S. J. van der Zant, "Single-molecule resonant tunneling diode," J. Phys. Chem. C **119**, 5697–5702 (2015).